

Cite this: *J. Mater. Chem. B*, 2020, **8**, 1914

## A distinctive mitochondrion-targeting, *in situ*-activatable near-infrared fluorescent probe for visualizing sulfur dioxide derivatives and their fluctuations *in vivo*†

Lintao Zeng,<sup>a</sup> Tianhong Chen,<sup>ab</sup> Bao-Quan Chen,<sup>b</sup> Hou-Qun Yuan,<sup>c</sup> Ruilong Sheng<sup>bd</sup> and Guang-Ming Bao<sup>bc</sup>

Sulfur dioxide derivatives are intimately involved in some physiological processes in organisms, and high levels of these substances can cause many diseases. Herein, we rationally prepared a mitochondrion-targeting, *in situ*-activatable near-infrared (NIR) fluorescent probe (**DCQN**) by coupling 2-(3,5,5-trimethylcyclohex-2-enylidene)malononitrile with 3-quinolinium carboxaldehyde. **DCQN** displayed a NIR fluorescence turn-on signal to indicate the presence of  $\text{HSO}_3^-$ , along with a considerable hyperchromic shift from light yellow to purple *via* a 1,4-nucleophilic addition reaction. We were able to use **DCQN** to instantaneously and quantitatively determine the concentration of  $\text{HSO}_3^-$  with high specificity, a low detection limit (24 nM), a large Stokes shift (~110 nm), and a high contrast ratio. Moreover, **DCQN** displayed good mitochondrion-targeting abilities and was *in situ*-activated by  $\text{HSO}_3^-$  to produce NIR fluorescence for imaging  $\text{HSO}_3^-$  in the mitochondria of live breast cancer cells. Furthermore, **DCQN** was used to monitor  $\text{HSO}_3^-$  in zebrafish with a high contrast ratio.

Received 18th November 2019,  
Accepted 28th January 2020

DOI: 10.1039/c9tb02593f

rsc.li/materials-b

### Introduction

Sulfur dioxide ( $\text{SO}_2$ ) in the atmosphere generally originates from the combustion of fossil fuels such as coal and petroleum.  $\text{SO}_2$  is colorless and can enter the body through the respiratory system and in this way pose a great threat to the health of organisms.<sup>1–4</sup> It becomes sulfite ( $\text{SO}_3^{2-}$ ) and bisulfite ( $\text{HSO}_3^-$ ) after being inhaled.<sup>5</sup> Exposure to high levels of  $\text{SO}_2$  has been shown to lead to serious diseases such as acute respiratory syndrome, cardiovascular disease, lung cancer, and neurological disorders.<sup>6–9</sup> In particular,  $\text{SO}_2$  and its derivatives can cause damage to mitochondria,<sup>10–12</sup> and such damage further triggers various sicknesses and dysfunctions<sup>13</sup> including cell malignancy, Alzheimer's disease, Parkinson's disease and atherosclerosis.<sup>14</sup> Thus, it is necessary to monitor the levels of  $\text{SO}_2$  derivatives in live organisms.<sup>15–19</sup>

Fluorescent probes have attracted great attention due to their high sensitivity and selectivity, ability to detect targets non-invasively, and fluorescence imaging.<sup>20–28</sup> To date, several fluorescent probes have been developed for sensing bisulfite based on various reaction mechanisms, including nucleophilic reactions of aldehydes,<sup>29,30</sup> selective deprotection of levulinate,<sup>31–33</sup> Michael-type additions<sup>34–36</sup> and coordinative interactions.<sup>37</sup> These probes efficiently detect bisulfite in food and live cells, but few of them have been effectively used for *in situ* sensing and imaging *in vivo*. The main obstacles are that these probes, being typically small molecules, often tend to diffuse across the cell membrane without targeting the mitochondria while endogenous  $\text{SO}_2$  derivatives are mainly generated within the mitochondria of live cells, some display short emission wavelength that cannot penetrate deep into tissues after reaction with bisulfite, and some are susceptible to nucleophilic reagents and enzymes (*e.g.*, esterases).<sup>38–40</sup> These drawbacks have inspired us to pursue the development of highly specific, rapid-response, mitochondrion-targeting *in situ*-activatable NIR fluorescent probes for imaging sulfur dioxide derivatives *in vivo*.<sup>41</sup>

Near-infrared (NIR) fluorescent probes offer a powerful tool to track and image some analytes *in vivo* by virtue of their low auto-fluorescence interference, their deep tissue-penetrability and the relatively little damage they inflict on biological samples.<sup>42,43</sup> In the current work, we designed and synthesized a mitochondrion-targeting and *in situ*-activatable NIR fluorescent

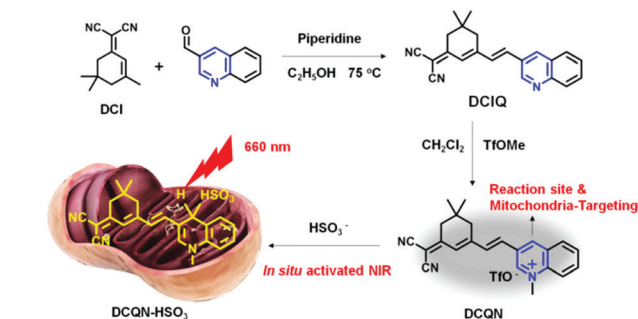
<sup>a</sup> College of Chemistry and Materials Science, Hubei Engineering University, Hubei, Xiaogan 432100, P. R. China. E-mail: zlt1981@126.com

<sup>b</sup> Tianjin Key Laboratory of Organic Solar Cells and Photochemical Conversion, Tianjin University of Technology, Tianjin, 300384, P. R. China

<sup>c</sup> School of Animal Science and Technology, Jiangxi Agricultural University, Nanchang 330045, P. R. China. E-mail: bycb2005@gmail.com

<sup>d</sup> CQM-Centro de Quimica da Madeira, Universidade da Madeira, Campus da Penteada, 9000-390, Funchal, Madeira, Portugal.  
E-mail: ruilong.sheng@staff.uma.pt; Fax: +351 291705254

† Electronic supplementary information (ESI) available: Experimental details and characterization data from the probe. See DOI: 10.1039/c9tb02593f



Scheme 1 Synthesis and working mechanism of the probe DCQN.

probe, DCQN, (Scheme 1) for imaging  $\text{HSO}_3^-$  *in vivo*. The quinolinium moiety of DCQN was shown to react with  $\text{HSO}_3^-$  via a 1,4-nucleophilic addition reaction to form product with a donor- $\pi$ -conjugation-acceptor (D- $\pi$ -A) structure, a feature that gave rise to an obvious chromogenic reaction and activated strong NIR fluorescence. Due to the high specificity and efficiency of this 1,4-nucleophilic addition, DCQN exhibited high selectivity and sensitivity, a low detection limit, and a rapid response to  $\text{HSO}_3^-$ . Furthermore, DCQN was effectively employed as a fluorescence imaging agent for monitoring  $\text{HSO}_3^-$  and its fluctuations in live breast cancer (MCF-7) cells and zebrafish.

## Results and discussion

### Design and synthesis of DCQN

In this work, we rationally designed a structurally simple, low-cost, near-infrared-light-emitting and highly water-soluble probe, namely DCQN, by coupling 2-(3,5,5-trimethylcyclohex-2-enylidene) malononitrile (DCI) with 3-quinolinecarboxaldehyde, followed by performing a methyl trifluoromethanesulfonate (TfOMe)-mediated methylation. DCQN was designed to contain two electron-withdrawing groups, namely 1-methylquinolinium and malononitrile groups, to form an acceptor- $\pi$ -conjugation-acceptor (A- $\pi$ -A) structure that could quench the fluorescence of the probe.<sup>44,45</sup> And the 4-position of methylquinolinium offered a potential reduction site for  $\text{HSO}_3^-$ . We set out to react DCQN with  $\text{HSO}_3^-$  in order to form an electron-rich enamine moiety, and hence resulting in a favorable D- $\pi$ -A structure and a typical intermolecular charge transfer (ICT) effect. Consequently, we observed an evident hyperchromic effect and NIR fluorescence “turn-on” emission with a large Stokes shift. DCQN was readily synthesized using conventional synthesis routes, as depicted in Scheme 1. The chemical structures of DCQN and its intermediates were confirmed using  $^1\text{H}$  NMR,  $^{13}\text{C}$  NMR and HRMS, as shown in ESI† (Fig. S8–S13).

### Spectral responses of DCQN towards $\text{HSO}_3^-$

The optical sensing of DCQN towards  $\text{HSO}_3^-$  was investigated using a DMSO/HEPES buffer solution ( $v/v = 1/9$ , 10 mM, pH 7.4) at 25 °C. As shown in Fig. 1(a), DCQN displayed a strong absorption peak at a wavelength of 380 nm. Upon addition of  $\text{HSO}_3^-$  (0–5 equiv.), the intrinsic absorption peak of DCQN at this wavelength gradually decreased, and a new peak at 550 nm

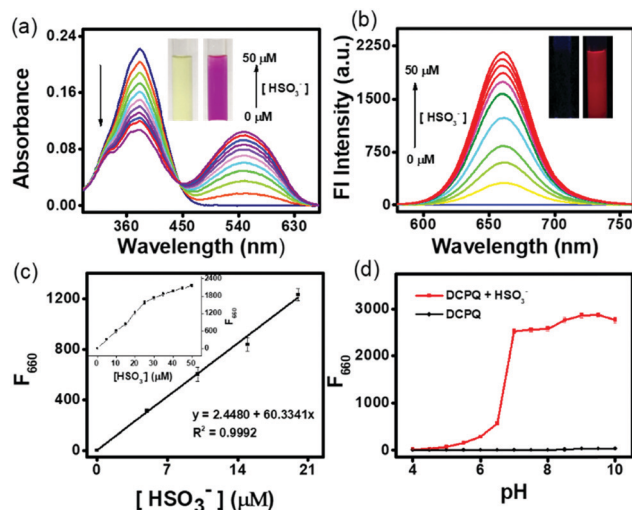


Fig. 1 (a) UV-vis absorption and (b) fluorescence spectra of DCQN (10  $\mu\text{M}$ ) in DMSO/HEPES buffer solution ( $v/v = 1/9$ , 10 mM, pH 7.4) with various amounts of added  $\text{HSO}_3^-$  (0–50.0  $\mu\text{M}$ ); inset: photographs of the DCQN solution before and after the addition of  $\text{HSO}_3^-$ . (c) The linear relationship between the fluorescence intensity of DCQN (10  $\mu\text{M}$ ) and the concentration of  $\text{HSO}_3^-$ . (d) Fluorescence response of DCQN (10  $\mu\text{M}$ ) to  $\text{HSO}_3^-$  (0.1 mM) in DMSO/HEPES solution ( $v/v = 1/9$ , 10 mM) at 25 °C as a function of pH. Each spectrum was recorded after incubation with  $\text{HSO}_3^-$  for 30 s. The excitation wavelength was 550 nm. Slits: 5/5 nm. The error bars represent  $\pm$  SD,  $n = 3$ .

emerged, affording an obvious hyperchromic shift from light yellow to purple. At the same time, a near-infrared fluorescence band at 660 nm ( $\Phi_f = 0.12$ ) was immediately observed with a large Stokes shift (Fig. 1b and Fig. S1, ESI†). This NIR fluorescent probe showed some merits such as high contrast ratio, relatively deep light penetration and low interference from background, and hence appeared to fully meet the requirements of imaging sulfur dioxide derivatives *in vivo*. Besides, a very highly linear correlation between fluorescence intensity ( $F_{660}$ ,  $R^2 = 0.9992$ ) and  $\text{HSO}_3^-$  concentration (0–20  $\mu\text{M}$ ) was observed (Fig. 1c), and the detection limit was 24 nM (Fig. S2, ESI†), suggesting that DCQN can be used to quantitatively detect  $\text{HSO}_3^-$  with high sensitivity. Since pH usually influences the sensing performances and chemical stabilities of probes, we investigated the fluorescence response of DCQN (10  $\mu\text{M}$ ) to 100  $\mu\text{M}$   $\text{HSO}_3^-$  in various pH conditions. As shown in Fig. 1(d), the fluorescence intensity ( $F_{660}$ ) of DCQN remained nearly constant within the pH range of 4–10. Whereas the addition of bisulfite (100  $\mu\text{M}$ ) triggered a sharp fluorescence enhancement at pH 6–10. These observations demonstrated that the good pH stability and applicability of the DCQN probe under pH 7.4, which endowed it with great potential for use in biological applications.

We also carried out a time-course investigation of the fluorescence response of DCQN (10  $\mu\text{M}$ ) to  $\text{HSO}_3^-$  (100  $\mu\text{M}$ ). As shown in Fig. 2,  $F_{660}$  of DCQN (10  $\mu\text{M}$ ) initially dramatically increased and then reached a plateau at about 6 s after the addition of  $\text{HSO}_3^-$  (10 equiv.), suggesting the ability of DCQN to serve as an ultra-rapidly responding fluorescent probe for imaging  $\text{HSO}_3^-$ .

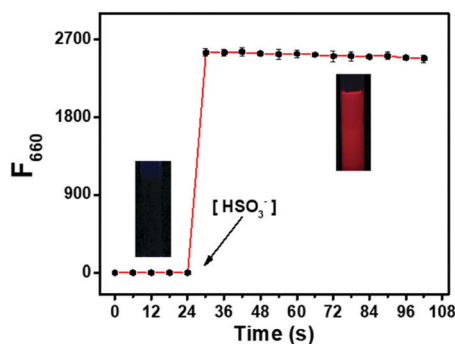


Fig. 2 Time course of the fluorescence response ( $F_{660}$ ) of DCQN (10  $\mu\text{M}$ ) to  $\text{HSO}_3^-$  (100.0  $\mu\text{M}$ ) in HEPES buffer solution (10 mM, pH 7.4, with 10% DMSO, v/v) at 25  $^\circ\text{C}$ . The excitation wavelength was 550 nm. Slits: 5/5 nm, the error bars represent  $\pm$  SD,  $n = 3$ .

### Analyte selectivity

Considering the complexity of the intracellular environment, a fluorescent probe with high selectivity is desired for accurate and real-time imaging of bisulfite in biological systems. To evaluate the selectivity of DCQN (10  $\mu\text{M}$ ) for  $\text{HSO}_3^-$  (100  $\mu\text{M}$ ), a variety of biological species (100  $\mu\text{M}$ ) were examined, including common anions ( $\text{Cl}^-$ ,  $\text{Br}^-$ ,  $\text{I}^-$ ,  $\text{HCO}_3^-$ ,  $\text{CO}_3^{2-}$ ,  $\text{AcO}^-$ ,  $\text{HPO}_4^{2-}$ ,  $\text{SO}_4^{2-}$ ,  $\text{S}_2\text{O}_3^{2-}$ ,  $\text{S}_2\text{O}_7^{2-}$ ,  $\text{SO}_3^{2-}$ ,  $\text{HS}^-$ , and  $\text{CN}^-$ ), nitroxides ( $\text{NO}_2^-$  and  $\text{NO}_3^-$ ), amines ( $\text{NH}_3\cdot\text{H}_2\text{O}$ ,  $\text{N}_2\text{H}_4\cdot\text{H}_2\text{O}$ , and  $n\text{-C}_3\text{H}_7\text{NH}_2$ ), reactive oxygen species ( $\text{ClO}^-$  and  $\text{H}_2\text{O}_2$ ) and bio-thiols (Cys, Hcy, and GSH). As shown in Fig. 3a, DCQN exhibited a negligible change in fluorescence and color upon the addition of any of test species except  $\text{HSO}_3^-$  and  $\text{SO}_3^{2-}$ . The addition of  $\text{HSO}_3^-$  or  $\text{SO}_3^{2-}$  caused an obvious hyperchromic shift from light yellow to purple together with a very strong enhancement of the fluorescence at 660 nm. Furthermore, we checked the selectivity of DCQN for  $\text{HSO}_3^-$  in the co-presence of other analytes. As shown in Fig. 3b, DCQN (10  $\mu\text{M}$ ) exhibited a remarkable fluorescence turn-on response to  $\text{HSO}_3^-$  (100  $\mu\text{M}$ ) even when any of various other anions and biological species (100  $\mu\text{M}$ ) was present. This finding indicated a high selectivity of the DCQN probe for  $\text{HSO}_3^-$  and that this probe might be effectively used in real biological systems.

### Mechanism of the DCQN sensing of $\text{HSO}_3^-$

To gain some information about the mechanism of the reaction between DCQN and  $\text{HSO}_3^-$ , we conducted  $^1\text{H}$  NMR titration experiments and HRMS analysis. As shown in Fig. 4, the proton chemical shifts of Ha and Hb in the quinolinium moiety appeared at 9.62 ppm and 9.27 ppm, respectively, and shifted to 6.42 ppm and 4.93 ppm after reaction with 18 equiv. of  $\text{HSO}_3^-$ . Meanwhile, the proton signal of Hc at 4.57 ppm assigned to the 1-position of the quinolinium moiety also shifted up-field (3.32 ppm). Analysis of the acquired  $^1\text{H}$  NMR spectra revealed that the quinolinium group of DCQN was attacked by  $\text{HSO}_3^-$ , followed by a C=C bond rearrangement to form DCQN- $\text{HSO}_3^-$  with a D- $\pi$ -A structure. The obtained HRMS results also confirmed the formation of the DCQN- $\text{HSO}_3^-$  adduct, as it showed a dominant peak at an  $m/z$  value of 420.1389 (calcd: 420.1387),

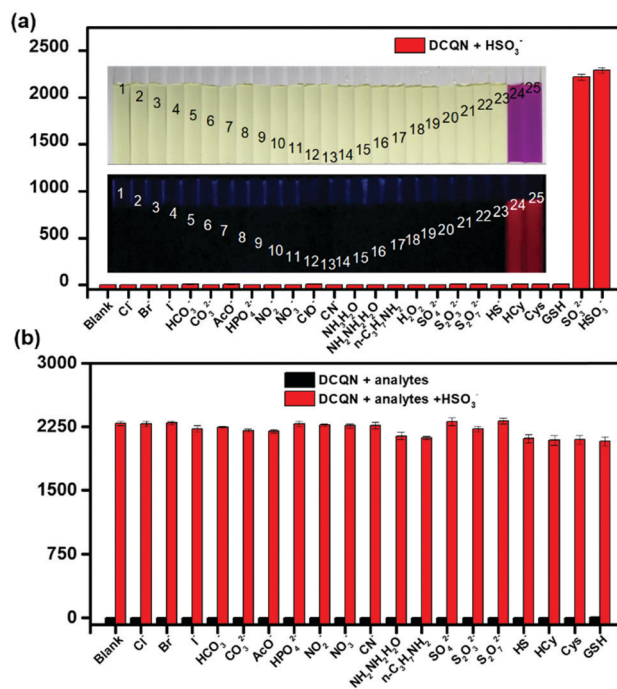


Fig. 3 Fluorescence responses of DCQN (10  $\mu\text{M}$ ) to various analytes (100.0  $\mu\text{M}$ ) in DMSO/HEPES buffer solution (v/v = 1/9, 10 mM, pH 7.4) at 25  $^\circ\text{C}$ . Each spectrum was recorded after 2 min. The excitation wavelength was 550 nm. Slits: 5/5 nm. Inset: Regular (upper) and fluorescence (bottom) photographs of DCQN (10  $\mu\text{M}$ ) in the presence of various species, specifically, from left to right: (1) blank, (2)  $\text{Cl}^-$ , (3)  $\text{Br}^-$ , (4)  $\text{I}^-$ , (5)  $\text{HCO}_3^-$ , (6)  $\text{CO}_3^{2-}$ , (7)  $\text{AcO}^-$ , (8)  $\text{HPO}_4^{2-}$ , (9)  $\text{NO}_2^-$ , (10)  $\text{NO}_3^-$ , (11)  $\text{ClO}^-$ , (12)  $\text{CN}^-$ , (13)  $\text{NH}_3\cdot\text{H}_2\text{O}$ , (14)  $\text{N}_2\text{H}_4\cdot\text{H}_2\text{O}$ , (15)  $n\text{-C}_3\text{H}_7\text{NH}_2$ , (16)  $\text{H}_2\text{O}_2$ , (17)  $\text{SO}_4^{2-}$ , (18)  $\text{S}_2\text{O}_3^{2-}$ , (19)  $\text{S}_2\text{O}_7^{2-}$ , (20)  $\text{HS}^-$ , (21) Hcy, (22) Cys, (23) GSH, (24)  $\text{SO}_3^{2-}$ , and (25)  $\text{HSO}_3^-$ . Error bars represent  $\pm$  SD,  $n = 3$ .

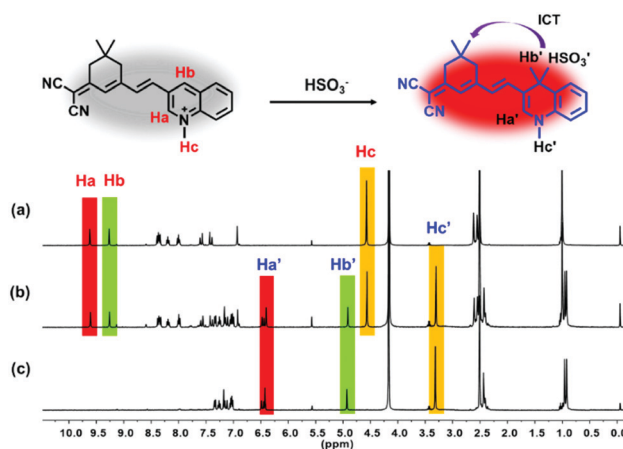


Fig. 4  $^1\text{H}$  NMR spectra of DCQN with (a) 0 equiv., (b) 9 equiv., and (c) 18 equiv. of  $\text{HSO}_3^-$ .

which corresponded to  $[\text{DCQN-HSO}_3\text{-H}]^-$  (Fig. S3, ESI $^\dagger$ ). These results were in good agreement with the spectral behavior of DCQN, and verified that DCQN exhibited a dramatic hyperchromic shift and near-infrared fluorescence light-up in response to  $\text{HSO}_3^-$  due to a 1,4-Michael reaction between the quinolinium skeleton and  $\text{HSO}_3^-$ .

### Cytotoxicity and fluorescence imaging for MCF-7 cells

Before DCQN was used to image  $\text{HSO}_3^-$  in MCF-7 cells, the cytotoxicity of DCQN was evaluated by performing a CCK-8 assay. As shown in Fig. 5, the cell survival rate remained above 87% after incubation with various concentrations of DCQN (0–25  $\mu\text{M}$ ) for 24 h, implying a good biocompatibility of DCQN. Encouraged by these favorable properties, we then utilized DCQN to image  $\text{HSO}_3^-$  in live MCF-7 cells. First, the MCF-7 cells were incubated with DCQN (10  $\mu\text{M}$ ) at 37 °C for 30 min and then fluorescence images of them were captured using laser confocal scanning microscopy. As shown in Fig. 6 and Fig. S4 (ESI<sup>†</sup>), MCF-7 cells were observed to be non-fluorescent in the red channel after incubation with DCQN for 30 min. Subsequently, these cells were incubated with  $\text{HSO}_3^-$  (0, 30 and 60  $\mu\text{M}$ ) for 10 min, and the images were recorded. Notably, these cells displayed clear red fluorescence cell profiles, and the fluorescence became much brighter as the concentration of  $\text{HSO}_3^-$  was increased. Notably, some albeit weak red fluorescence was observed in the cells incubated with DCQN and then  $\text{HSO}_3^-$  at a concentration as low as 250 nM (Fig. S5, ESI<sup>†</sup>), suggesting that DCQN could serve as a sensitive probe for efficiently imaging exogenous  $\text{HSO}_3^-$  in live cells. DCQN also displayed good optical stability in the live cells (shown in Fig. S6, ESI<sup>†</sup>). Thus, this NIR-light-emitting fluorescent probe was found to display several advantages such as good photostability, high contrast ratio and low background interference, which are favorable for imaging  $\text{HSO}_3^-$  *in vivo*.

### Fluorescence imaging of $\text{HSO}_3^-$ located in mitochondria

$\text{SO}_2$  derivatives also can be endogenously generated within mitochondria. To explore the mitochondria targeting and sensing ability of DCQN for  $\text{HSO}_3^-$ , MCF-7 cells were co-incubated with DCQN (10  $\mu\text{M}$ ) and the commercially available Mito-Tracker Green (200 nM) at 37 °C for 30 min. Afterwards, they were further incubated with  $\text{HSO}_3^-$  (60  $\mu\text{M}$ ) for another 10 min and their fluorescence images were recorded by using a confocal laser-scanning microscope. As shown in Fig. 7, we observed very clear red fluorescence profiles of mitochondria in the MCF-7 cells pre-incubated first with DCQN and then  $\text{HSO}_3^-$  (60  $\mu\text{M}$ ). The fluorescence co-localization of Mito-Tracker Green and DCQN overlapped essentially perfectly, and the corresponding Pearson's correlation coefficient was 0.95. Hence, DCQN was

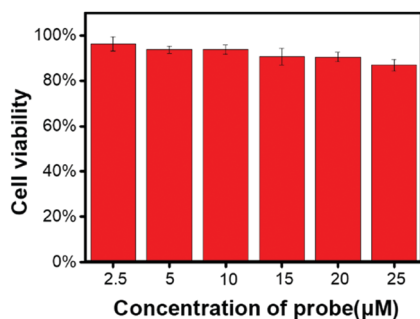


Fig. 5 MCF-7 cell viabilities after incubation with various concentrations of DCQN (0–25  $\mu\text{M}$ ) for 24 h. Error bars represent  $\pm$  SD,  $n = 5$ .

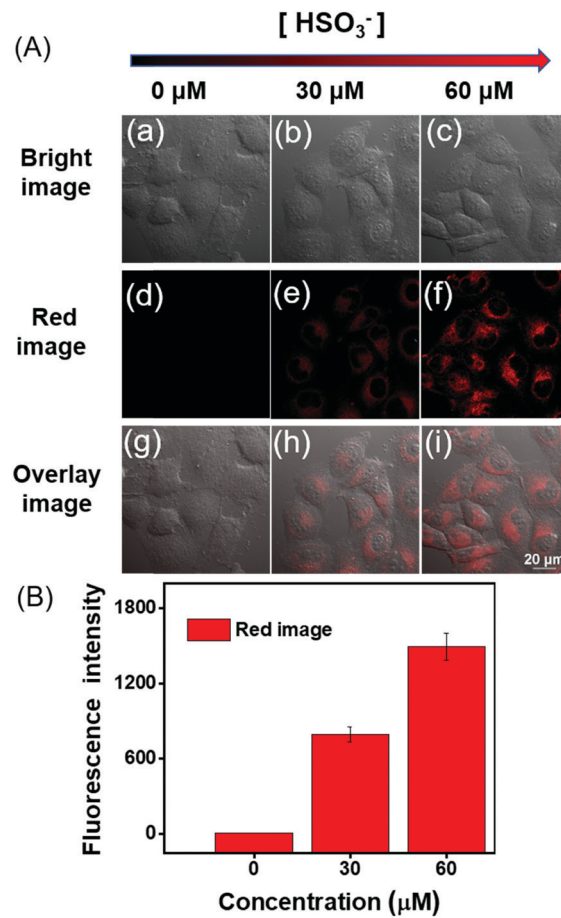


Fig. 6 (A) Confocal images of various samples of MCF-7 cells incubated with DCQN (10  $\mu\text{M}$ ) at 37 °C for 30 min, and then treated with different concentrations of  $\text{HSO}_3^-$  (0–60  $\mu\text{M}$ ) for 10 min. Cell images were acquired with  $\lambda_{\text{ex}}/\lambda_{\text{em}}$  of 543/648–703 nm. Scale bar: 20  $\mu\text{m}$ . (B) Statistical analysis based on the peak fluorescence intensity of MCF-7 cells. Error bars represent  $\pm$  SD,  $n = 5$ .

found to display an excellent mitochondrion-targeting ability and could be activated by exogenous bisulfite to generate NIR fluorescence inside mitochondria of live cells.

### Fluorescence imaging of $\text{HSO}_3^-$ in zebrafish

In view of the above-described meritorious characteristics of DCQN, we further exploited the capability of DCQN for the fluorescence imaging of  $\text{HSO}_3^-$  *in vivo*. Zebrafish was used as the vertebrate organism to perform fluorescence imaging of  $\text{HSO}_3^-$  *in vivo*. As shown in Fig. 8, the zebrafish did not fluoresce when they were incubated with just DCQN (10  $\mu\text{M}$ ) for 30 min. These zebrafish were further incubated with different concentrations of  $\text{HSO}_3^-$  (0, 30, 60, 90 and 120  $\mu\text{M}$ ) for 10 min at 28 °C and images of them were acquired with a confocal laser-scanning microscopy. As expected, red fluorescence appeared within the zebrafish when  $\text{HSO}_3^-$  was included, and the fluorescence intensity became much stronger (red channel with  $\lambda_{\text{ex}}/\lambda_{\text{em}}$  of 543/648–703 nm) as the  $\text{HSO}_3^-$  concentration was increased from 0 to 120  $\mu\text{M}$ . The red fluorescence was mainly located at the contours of the eyes and abdomen (Fig. 8, enlarged red images), and became much

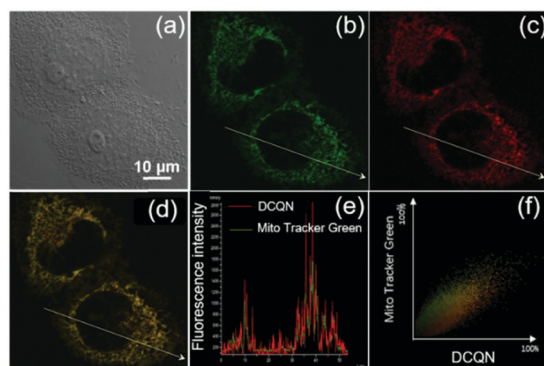


Fig. 7 Confocal images of MCF-7 cells stained with (b) 200  $\mu\text{M}$  Mito Tracker Green (green channel  $\lambda_{\text{ex}}/\lambda_{\text{em}}$  of 488/500–530 nm) and (c) 10  $\mu\text{M}$  DCQN (red channel  $\lambda_{\text{ex}}/\lambda_{\text{em}}$  of 543/648–703 nm) for 30 min and then further incubated with  $\text{HSO}_3^-$  (60  $\mu\text{M}$ ) for another 10 min in MCF-7 cells. (a) Bright images, (d) merged images, (e) intensity profile within the regions of interest, and (f) a correlation plot of Mito-Tracker Green and DCQN intensities. Pearson's correlation coefficient: 0.95. Scale bar: 10  $\mu\text{m}$ .

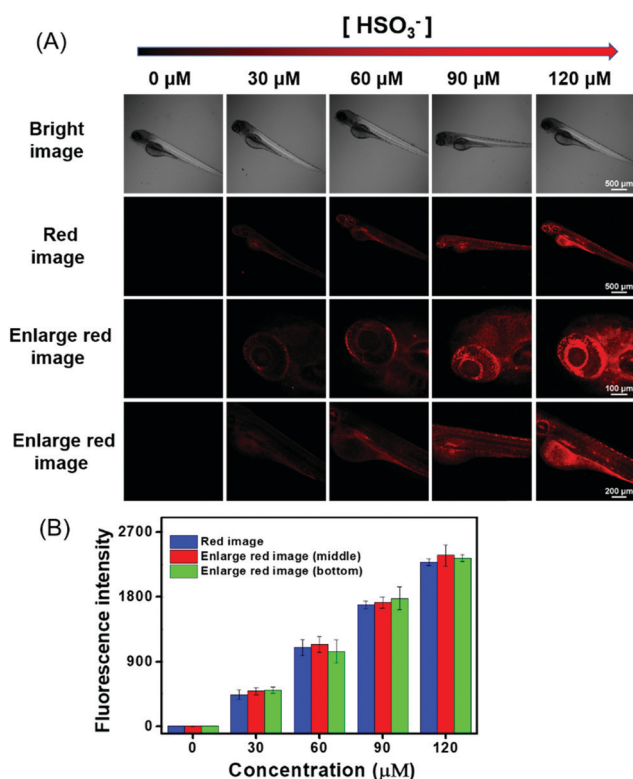


Fig. 8 (A) Confocal images of various four-day-old zebrafish pre-incubated with DCQN (10  $\mu\text{M}$ ) at 28  $^\circ\text{C}$  for 30 min, and then treated with different concentrations of  $\text{HSO}_3^-$  (0, 30, 60, 90, 120  $\mu\text{M}$ ) for 10 min. These images were acquired with  $\lambda_{\text{ex}}$  of 543 nm and emission wavelength between 648 and 703 nm. Scale bar: 500  $\mu\text{m}$ . The local merged scale bar: 200  $\mu\text{m}$  and 100  $\mu\text{m}$ . (B) Statistical analysis based on peak fluorescence intensity of the zebrafish. Error bars represent  $\pm$  SD,  $n = 5$ .

brighter here with the increase in  $\text{HSO}_3^-$  concentration. Hence, DCQN could be used to track bisulfite in living system. To further demonstrate the excellent imaging ability of DCQN, the zebrafish were first incubated with DCQN (10  $\mu\text{M}$ ) for 30 min,

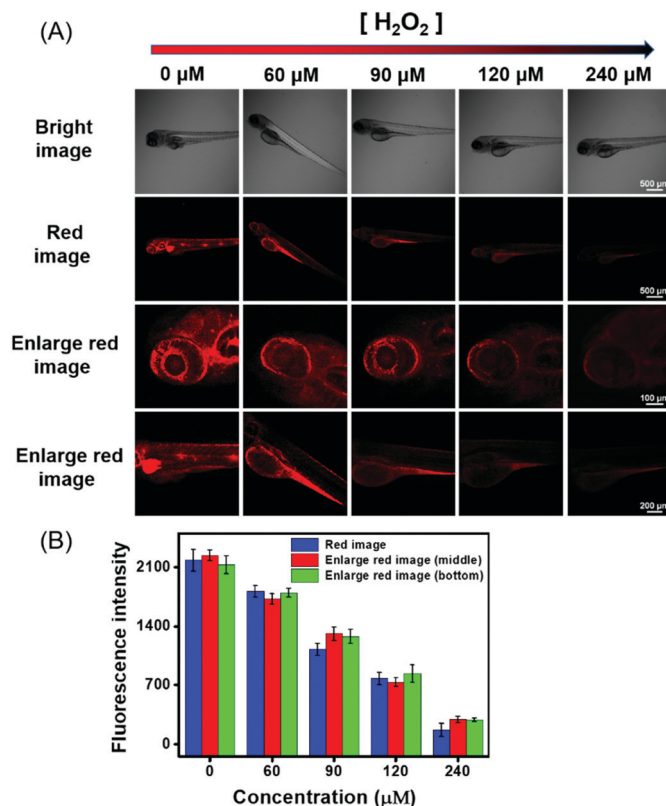


Fig. 9 (A) Confocal images of four-day-old zebrafish loaded with DCQN (10  $\mu\text{M}$ ) at 28  $^\circ\text{C}$  for 30 min, followed by being incubated with  $\text{HSO}_3^-$  (120  $\mu\text{M}$ ) for 10 min, and then with different concentrations of  $\text{H}_2\text{O}_2$  (0, 60, 90, 120, and 240  $\mu\text{M}$ ) for 10 min at 28  $^\circ\text{C}$ . These images were acquired with  $\lambda_{\text{ex}}$  of 543 nm and emission wavelengths between 648 and 703 nm. Scale bar: 500  $\mu\text{m}$ . The local merged scale bars were 200  $\mu\text{m}$  and 100  $\mu\text{m}$ , respectively. (B) Statistical analysis based on the peak fluorescence intensity of the zebrafish. Error bars represent  $\pm$  SD,  $n = 5$ .

then stimulated with  $\text{HSO}_3^-$  (120  $\mu\text{M}$ ) for 10 min, and finally treated with different concentrations of  $\text{H}_2\text{O}_2$  (0, 60, 90, 120 and 240  $\mu\text{M}$ ) for another 10 min, after which fluorescence images of these zebrafish were recorded. As shown in Fig. 9, while very strong red fluorescence was observed within the zebrafish incubated with just DCQN and  $\text{HSO}_3^-$ , the intensity of the fluorescence decreased as the  $\text{H}_2\text{O}_2$  concentration was increased from (0 to 240  $\mu\text{M}$ ), which again confirmed the good imaging ability of DCQN. Moreover, these observations implied that the  $\text{SO}_2$  derivative and DCQN- $\text{HSO}_3^-$  could be oxidized by  $\text{H}_2\text{O}_2$ . Hence, according to our results, DCQN can be employed as an *in vivo* NIR imaging agent to visually study the process of the detoxification of sulfur dioxide derivatives with oxidants. Further research about this function is expected to be carried out in the near future.

### *In vivo* fluorescence imaging of $\text{HSO}_3^-$ during the growth and development of zebrafish

Sulfur dioxide derivatives have been previously shown to cause oxidative damage to living organisms.<sup>46,47</sup> Herein, we further explored the absorption of  $\text{HSO}_3^-$  and its distribution in the body during the growth and development of zebrafish.

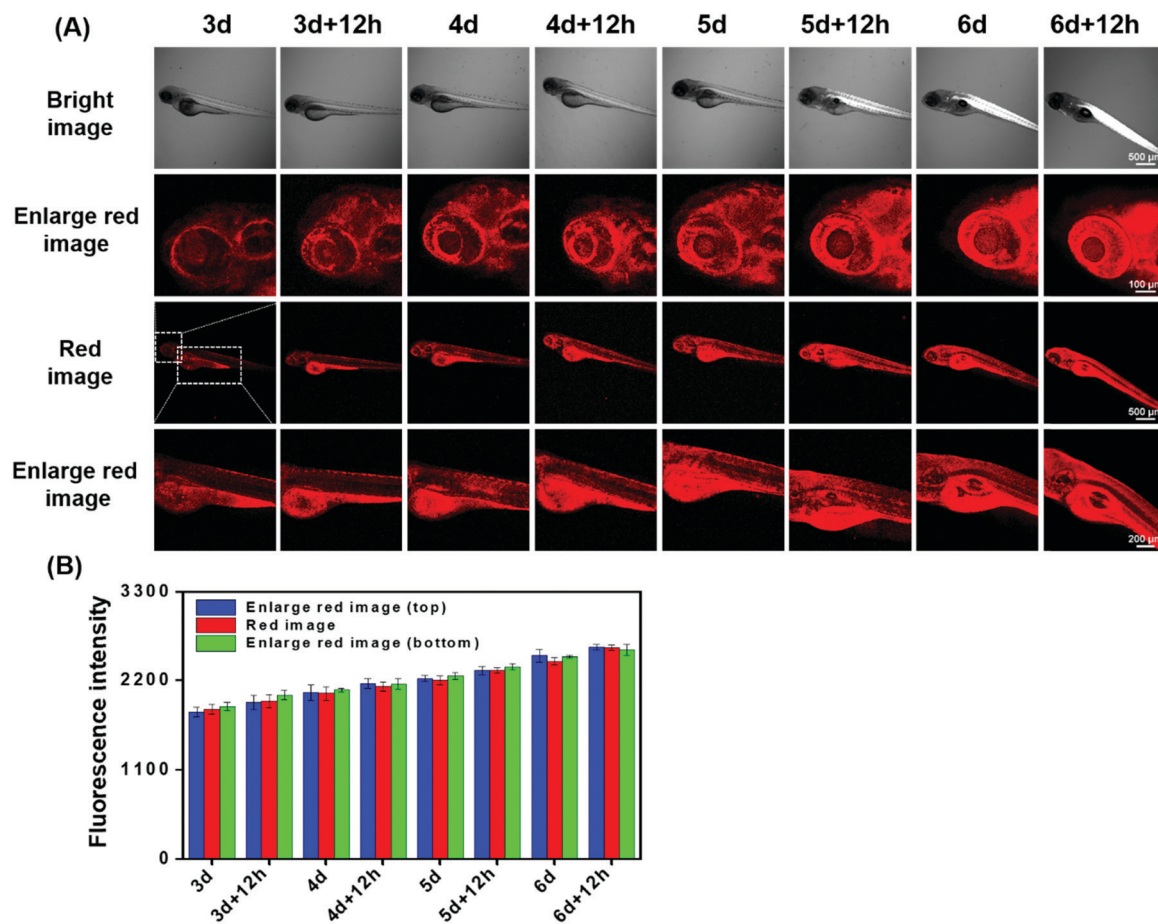


Fig. 10 (A) Confocal images of different zebrafish incubated with DCQN (10 μM) at 28 °C for 30 min, and then treated with HSO<sub>3</sub><sup>-</sup> (120 μM) for 10 min. These images were acquired with λ<sub>ex</sub> of 543 nm and emission wavelengths between 648 and 703 nm. Scale bar: 500 μm. The partial imaging scale bar: 200 μm and 100 μm. (B) Statistical analysis based on the peak fluorescent intensity of the zebrafish. Error bars represent ± SD, n = 5.

Zebrafish between three and six days of age were pre-incubated with DCQN (10 μM) for 30 min at 28 °C, and further treated with HSO<sub>3</sub><sup>-</sup> (120 μM) for 10 min. As shown in Fig. 10, bright red fluorescence in the entire body of zebrafish was boosted by HSO<sub>3</sub><sup>-</sup>. This result implied that HSO<sub>3</sub><sup>-</sup> can quickly enter and spread throughout the whole body, and hence subsequently possibly cause systemic oxidation-associated injury. Interestingly, red fluorescence (shown in Fig. 10, enlarged red image) was much brighter at the head, intestines and abdomen than at other body parts. This result indicated that sulfur dioxide derivatives would tend to accumulate in these organs and may subsequently damage them, thereby causing local pathological changes. Also, the fluorescence intensity in the zebrafish became much stronger as the culture time was prolonged. To our delight, we clearly observed the development of the eyeballs, abdomen and head. Apparently, various organs of the zebrafish gradually matured and showed their morphologies in the presence of HSO<sub>3</sub><sup>-</sup> (120 μM) (Fig. S7, ESI†). The fluorescence enhancement with increased growth time may be attributed to the enhancement of the digestion and absorption functions of the zebrafish. The results demonstrated that DCQN could be employed to visibly monitor the absorption and distribution of HSO<sub>3</sub><sup>-</sup> in zebrafish during their growth and development period.

## Experimental

### Materials and characterizations

Unless specifically indicated, all reagents were supplied by Heowns-Reagent and Sigma-Aldrich, and used without further purification. <sup>1</sup>H and <sup>13</sup>C NMR spectra were acquired by using a Bruker AV spectrometer with tetramethylsilane (TMS) as an internal standard. High-resolution mass spectra (HRMS) were recorded by using an HP-1100 LC-MS spectrometer. UV-Vis absorption spectra were acquired by using a Hitachi UV-3310 spectrometer.

Fluorescence spectra were acquired by using a Hitachi FL-4500 fluorometer. Confocal fluorescence microscopy images of MCF-7 cells were acquired by using a Nikon A1 laser-scanning confocal microscope with a 100× objective lens (numerical aperture of the objective: 100×/1.4 oil (DIC N2), OFN, Plan Apo VC, Nikon Company; immersion oil, type: NF, nd = 1.515 (23 °C); microscope: Ti microscope, light path: L100, condenser: 3 (DIC N2)). Confocal fluorescence microscopy images of zebrafish were acquired by using a Nikon A1 laser-scanning confocal microscope with 4× objective lens (numerical aperture of the objective: 4×/0.2 dry (DIC N2), OFN, Plan Apo, Nikon Company).

### Synthesis of DCIQ

DCI (300 mg, 1.61 mmol), which was prepared according to the literature,<sup>48</sup> along with 3-quinolinecarboxaldehyde (276 mg, 1.76 mmol), piperidine (25  $\mu$ L, 0.25 mmol) and 25 mL anhydrous ethanol were refluxed for 7 h under an N<sub>2</sub> atmosphere. Then, the reaction mixture was cooled down, and the solvent was evaporated using a rotary evaporator. The residual mixture was purified by performing silica gel chromatography (eluent: CH<sub>2</sub>Cl<sub>2</sub>/ethanol = 60/1, v/v) to give the yellow solid DCIQ (323 mg, yield: 68%). <sup>1</sup>H NMR (400 MHz, DMSO-*d*<sub>6</sub>)  $\delta$  9.25 (s, 1H), 8.65 (s, 1H), 8.04–8.02 (d, *J* = 8.0 Hz, 1H), 7.99–7.79 (d, *J* = 8.0 Hz, 1H), 7.81–7.77 (t, *J* = 8.0 Hz, 1H), 7.76–7.72 (d, *J* = 16.0 Hz, 1H), 7.67–7.63 (t, *J* = 8.0 Hz, 1H), 7.52–7.48 (d, *J* = 16.0 Hz, 1H), 6.98 (s, 1H), 2.66 (s, 2H), 2.61 (s, 2H), 1.05 (s, 6H). <sup>13</sup>C NMR (100 MHz, DMSO-*d*<sub>6</sub>)  $\delta$  170.7, 155.7, 150.5, 147.9, 134.6, 131.9, 129.7, 129.6, 129.3, 129.0, 128.0, 127.8, 124.1, 114.2, 113.4, 77.7, 42.7, 38.5, 32.2, 27.9. HRMS(ESI): *m/z*: [M + H]<sup>+</sup> calcd for C<sub>22</sub>H<sub>20</sub>N<sub>3</sub>: 326.1657; found: 326.1669.

### Synthesis of DCQN

DCIQ (200 mg, 614.6  $\mu$ mol), methyl trifluoromethanesulfonate (278 mL, 2.46 mmol) and 15 mL of dry dichloromethane were stirred for 12 h at ambient conditions. The reaction solution was concentrated to 1 mL by using a rotary evaporator, and then poured into a flask containing 10 mL of *n*-hexane to precipitate the yellow solid DCQN (412 mg, yield: 85%). <sup>1</sup>H NMR (400 MHz, DMSO-*d*<sub>6</sub>)  $\delta$  9.90 (s, 1H), 9.40 (s, 1H), 8.52–8.50 (d, *J* = 8.0 Hz, 1H), 8.41–8.39 (d, *J* = 8.0 Hz, 1H), 8.30–8.25 (t, *J* = 10.0 Hz, 1H), 8.09–8.05 (t, *J* = 8.0 Hz, 1H), 7.80–7.76 (d, *J* = 16.0 Hz, 1H), 7.55–7.51 (d, *J* = 16.0 Hz, 1H), 6.97 (s, 1H), 4.64 (s, 3H), 2.70 (s, 2H), 2.60 (s, 2H), 1.07 (s, 6H). <sup>13</sup>C NMR (100 MHz, DMSO-*d*<sub>6</sub>)  $\delta$  170.4, 154.1, 143.7, 137.9, 136.0, 134.9, 131.0, 130.7, 129.4, 125.6, 122.7, 119.8, 119.5, 113.8, 113.2, 79.5, 46.2, 38.5, 32.2, 27.9. HRMS (ESI): *m/z*: [M]<sup>+</sup> calcd for C<sub>24</sub>H<sub>22</sub>F<sub>3</sub>N<sub>3</sub>O<sub>3</sub>S: 340.1808; found: 340.1811.

### Cell cultures and fluorescence imaging

MCF-7 cells were cultured in Dulbecco's modified Eagle's medium (DMEM) supplemented with 10% fetal bovine serum (FBS, Invitrogen Corp., Carlsbad, CA) and penicillin–streptomycin (100 units per ml of penicillin and 100  $\mu$ g per ml of streptomycin, Invitrogen Corp., Carlsbad, CA) at 37 °C in an incubator of air with 5% CO<sub>2</sub> and constant humidity. Before each imaging experiment was carried out, MCF-7 cells (2  $\times$  10<sup>4</sup> cells per mL) were seeded in a 35 mm glass bottom dish (D110100, Matsunami, Japan) for 24 h. DCQN (10  $\mu$ M) was added to the MCF-7 cells and incubated for 30 min at 37 °C. After that, the sample to be imaged was washed with PBS buffer (pH = 7.4) three times to remove the residual DCQN. Then to each sample of cells was added a different concentration of HSO<sub>3</sub><sup>−</sup> (0, 30, 60  $\mu$ M), and the resulting samples were incubated for 10 min, after which fluorescence images were acquired of them using a Nikon A1 confocal laser-scanning microscope.

### Fluorescence imaging in zebrafish

Three-day post-fertilization zebrafish were purchased from Nanjing EzeRinka Biotechnology Co., Ltd. These zebrafish were

cultured at 28 °C in the embryo medium supplemented with 1-phenyl-2-thiourea (PTU). To explore the performance of DCQN for imaging HSO<sub>3</sub><sup>−</sup> in the 4-day old zebrafish, samples of these zebrafish were incubated with embryo medium containing DCQN (10  $\mu$ M) for 30 min. Then, they were washed with embryo medium three times, and further incubated with HSO<sub>3</sub><sup>−</sup> solution (0, 30, 60, 90, 120  $\mu$ M) for 10 min. All zebrafish samples were washed three times with embryo medium before being imaged using a Nikon A1 confocal laser – scanning microscope. To determine HSO<sub>3</sub><sup>−</sup> levels arising from the process of H<sub>2</sub>O<sub>2</sub>-induced oxidative stress, a control fluorescence imaging experiment involving H<sub>2</sub>O<sub>2</sub> was also carried out. First, the zebrafish samples were incubated with DCQN (10  $\mu$ M) for 30 min and then treated with HSO<sub>3</sub><sup>−</sup> (120  $\mu$ M) for 10 min. Then they were incubated with different concentrations (60, 90, 120, 240  $\mu$ M) of H<sub>2</sub>O<sub>2</sub> for 10 min at 28 °C. All zebrafish samples were washed three times with embryo medium and then images of them were acquired with a Nikon A1 confocal laser – scanning microscope.

## Conclusions

In conclusion, a highly specific, rapidly responsive, mitochondrion-targeting near-infrared fluorescent probe, DCQN, was rationally prepared for the *in situ* monitoring of HSO<sub>3</sub><sup>−</sup> *in vivo*. DCQN could be used to determine the concentration of HSO<sub>3</sub><sup>−</sup> with high sensitivity (detection limit of 24 nM), a large Stokes shift (~110 nm) and a very rapid response (6 s). Moreover, DCQN was indicated to be quite biocompatible and was successfully used to image exogenous HSO<sub>3</sub><sup>−</sup> in the mitochondria of live breast cancer (MCF-7) cells with large NIR fluorescence enhancement and a high contrast ratio. Moreover, DCQN was successfully used to image HSO<sub>3</sub><sup>−</sup> in zebrafish with activated NIR emission during their growth and development processes (3–6 days). The excellent NIR emission, rapid response and *in situ*-activatable fluorescence features make DCQN an ideal imaging agent for visualizing sulfur dioxide derivatives in live organisms.

## Conflicts of interest

All authors of this work declare no research conflicts.

## Acknowledgements

This work was sponsored by the National Natural Science Foundation of China (No. 21978222, 31960720, 31560712), and the Natural Science Foundation of Tianjin (No. 17JCYBJC19600, 18JCYBJC94900). Ruilong Sheng appreciates support from Fundação para a Ciência e a Tecnologia (FCT project PEst-OE/QUI/UI0674/2019, CQM, Portuguese government funds), ARDITI-Agência Regional para o Desenvolvimento da Investigação Tecnologia e Inovação through the project M1420-01-0145-FEDER-000005-Centro de Química da Madeira-CQM+ (Madeira 14-20 Program) and ARDITI-2017-ISG-003.

## Notes and references

- 1 K. K. Bertine and E. D. Goldberg, *Science*, 1971, **173**, 233–235.
- 2 W. Chen, Q. Fang, D. Yang and X. J. Foley, *Anal. Chem.*, 2015, **87**, 609–616.
- 3 A. Heagle, D. Body and W. W. Heck, *J. Environ. Qual.*, 1973, **2**, 365–368.
- 4 N. Sang, Y. Yun, H. Li, L. Hou, M. Han and G. Li, *Toxicol. Sci.*, 2010, **114**(2), 226–236.
- 5 X. Shi, *J. Inorg. Biochem.*, 1994, **56**, 155–165.
- 6 T. Finkel and N. J. Holbrook, *Nature*, 2000, **408**, 239–247.
- 7 Y. Sun, J. Liu, J. Zhang, T. Yang and W. Guo, *Chem. Commun.*, 2013, **49**(26), 2637–2639.
- 8 J. Xu, J. Pan, X. Jiang, C. Qin, L. Zeng, H. Zhang and J. F. Zhang, *Biosens. Bioelectron.*, 2016, **77**, 725–732.
- 9 W. Zhang, T. Liu, F. Huo, P. Ning, X. Meng and C. Yin, *Anal. Chem.*, 2017, **89**(15), 8079–8083.
- 10 H. Jin, A. Liu, L. Holmberg, M. Zhao, S. Chen, J. Yang, Y. Sun, S. Chen, C. Tang and J. Du, *Int. J. Mol. Sci.*, 2013, **14**, 10465–10482.
- 11 G. Fang, X. Yang, W. Wang, Y. Feng, W. Zhang, Y. Huang, C. Sun, M. Chen and X. Meng, *Sens. Actuators, B*, 2019, **297**, 126777.
- 12 G. Chen, W. Zhou, C. Zhao, Y. Liu, T. Chen, Y. Li and B. Tang, *Anal. Chem.*, 2018, **90**, 12442–12448.
- 13 S. W. Tait and D. R. Green, *Nat. Rev. Mol. Cell Biol.*, 2010, **11**, 621–632.
- 14 K. Luby-Phelps, *Int. Rev. Cytol.*, 1999, **192**, 189–221.
- 15 W. Xu, C. L. Teoh, J. Peng, D. Su, L. Yuan and Y. T. Chang, *Biomaterials*, 2015, **56**, 1–9.
- 16 D. P. Li, Z. Y. Wang, X. J. Cao, J. Cui, X. Wang, H. Z. Cui, J. Y. Miao and B.-X. Zhao, *Chem. Commun.*, 2016, **52**, 2760–2763.
- 17 L. Yuan, W. Lin, J. Song and Y. Yang, *Chem. Commun.*, 2011, **47**, 12691–12693.
- 18 Y. Yang, L. He, K. Xu and W. Lin, *Anal. Methods*, 2019, **11**, 3931–3935.
- 19 Y. Yan, X. He, J. Miao and B.-X. Zhao, *J. Mater. Chem. B*, 2019, **7**, 6585–6591.
- 20 L. Yuan, W. Lin, Y. Xie, B. Chen and J. Song, *Chem. – Eur. J.*, 2012, **18**, 2700–2706.
- 21 D. Cheng, Y. Pan, L. Wang, Z. Zeng, L. Yuan, X. Zhang and Y. T. Chang, *J. Am. Chem. Soc.*, 2017, **139**, 285–292.
- 22 Z. Ye, C. Duan, R. Sheng, J. Xu, H. Wang and L. Zeng, *Talanta*, 2018, **176**, 389–396.
- 23 J. Xu, H. Yuan, L. Zeng and G. Bao, *Chin. Chem. Lett.*, 2018, **29**, 1456–1464.
- 24 M.-Y. Wu, K. Li, C.-Y. Li, J.-T. Hou and X.-Q. Yu, *Chem. Commun.*, 2014, **50**(2), 183–185.
- 25 J. Wu, J. Pan, Z. Ye, L. Zeng and D. Su, *Sens. Actuators, B*, 2018, **274**, 274–284.
- 26 Y. Zhao, Y. Ma and W. Lin, *Sens. Actuators, B*, 2018, **268**, 157–163.
- 27 C. Duan, M. Won, P. Verwilt, J. Xu, H. Kim, L. Zeng and J. Kim, *Anal. Chem.*, 2019, **96**, 4172–4178.
- 28 J.-T. Hou, H. Kim, C. Duan, M. Ji, S. Wang, L. Zeng, W. Ren and J. Kim, *Chem. Commun.*, 2019, **55**, 2533–2536.
- 29 X. Cheng, H. Jia, J. Feng, J. Qin and Z. Li, *Sens. Actuators, B*, 2013, **184**, 274–280.
- 30 C. Yin, X. Li, Y. Yue, J. Chao, Y. Zhang and F. Huo, *Sens. Actuators, B*, 2017, **246**, 615–622.
- 31 X. Ma, C. Liu, Q. Shan, G. Wei, D. Wei and Y. Du, *Sens. Actuators, B*, 2013, **188**, 1196–1200.
- 32 M. G. Choi, J. Hwang, S. Eor and S.-K. Chang, *Org. Lett.*, 2010, **12**, 5624–5627.
- 33 S. Chen, P. Hou, J. Wang and X. Song, *RSC Adv.*, 2012, **2**, 10869–10873.
- 34 Y. Liu, K. Li, K.-X. Xie, L.-L. Li, K.-K. Yu, X. Wang and X.-Q. Yu, *Chem. Commun.*, 2016, **52**(16), 3430–3433.
- 35 W.-L. Wu, H.-L. Ma, M.-F. Huang, J.-Y. Miao and B.-X. Zhao, *Sens. Actuators, B*, 2017, **241**, 239–244.
- 36 C. Duan, J. Zhang, Y. Hu, L. Zeng, D. Su and G.-M. Bao, *Dyes Pigm.*, 2019, **162**, 459–465.
- 37 Y. Sun, C. Zhong, R. Gong, H. Mu and E. Fu, *J. Org. Chem.*, 2009, **74**, 7943–7946.
- 38 L. Tang, P. He, X. Yan, J. Sun, K. Zhong, S. Hou and Y. Bian, *Sens. Actuators, B*, 2017, **247**, 421–427.
- 39 Q. Sun, W. Zhang and J. Qian, *Talanta*, 2017, **162**, 107–113.
- 40 Y. Liu, J. Nie, J. Niu, W. Wang and W. Lin, *J. Mater. Chem. B*, 2018, **6**(13), 1973–1983.
- 41 H. Agarwalla, S. Pal, A. Paul, Y. W. Jun, J. Bae, K. H. Ahn, D. N. Srivastava and A. Das, *J. Mater. Chem. B*, 2016, **4**, 7888–7894.
- 42 W. Zhang, F. Huo, Y. Zhang, J. Chao and C. Yin, *Sens. Actuators, B*, 2019, **297**, 126747.
- 43 L. Yuan, W. Lin, K. Zheng, L. He and W. Huang, *Chem. Soc. Rev.*, 2013, **42**, 622–661.
- 44 G. Yeap, E. Hrishikesan and Y. Chan, *J. Fluoresc.*, 2017, **27**, 105–110.
- 45 J.-H. Jeonga, J.-S. Kim, J. Campob, S.-H. Leea, W.-Y. Jeona, W. Wenseleersb, M. Jazbinsek, H. Yund and O.-P. Kwona, *Dyes Pigm.*, 2015, **113**, 8–17.
- 46 Z. Meng, B. Zhang, J. Bai, H. Geng and C. Liu, *Inhalation Toxicol.*, 2003, **15**, 397–410.
- 47 Z. Meng, R. Li and X. Zhang, *Inhalation Toxicol.*, 2005, **17**, 309–313.
- 48 Z. Gao, X. Zhang, M. Zheng and Y. Chen, *Dyes Pigm.*, 2015, **120**, 37–43.